

Amplitude and Frequency encodings give cells a different lens to sense the environment.

Alan Givré¹, Alejandro Colman-Lerner² and Silvina Ponce Dawson¹

¹UBA, FCEN, Departamento de Física and CONICET-UBA, IFIBA,

²UBA, FCEN, Departamento de Fisiología, Biología Molecular y Celular and CONICET-UBA, IFIBYNE, Ciudad Universitaria, (1428) Buenos Aires, Argentina

Cells continuously sense their surroundings to detect modifications and generate responses. Very often changes in extracellular concentrations initiate *signaling cascades* that eventually result in changes in gene expression. Increasing stimulus strengths can be encoded in increasing concentration amplitudes or increasing activation frequencies of intermediaries of the pathway. In this Letter we show how the different way in which *amplitude* and *frequency* encoding map environmental changes impact on the cell's information transmission capabilities. While amplitude encoding is optimal for a limited range of stimuli strengths around a finite value, frequency encoding information transmission can improve or remain relatively flat as the stimulus strength increases. The apparently redundant combination of both mechanisms in some cell types may then serve the purpose of expanding the range over which stimulus strengths can be reliably discriminated. In this Letter we also discuss a possible example of this mechanism.

Cells continuously sense their surroundings to detect modifications and generate appropriate responses. Environmental changes are often due to changes in concentrations which induce further changes in intracellular components producing a *signaling cascade*. There are different strategies that cells use to “interpret” and react to environmental changes. On occasions, the intensity of the external stimulus is encoded in the *amplitude* of the concentration of active molecules in the following steps of the signaling pathway [1–3]. In others, it is encoded in the *frequency* with which the molecules of one or more steps switch between being active and inactive[4–7]. When the end response involves modifications of gene expression these different strategies may result in different dynamics of transcription factor (TF) nuclear fractions which can remain elevated for a certain time or display pulsatile behavior [6–9]. The question then arises of how the two types of encoding differ and under what circumstances one of them could be better suited than the other [6, 10–12]. The studies of [7, 13, 14] showed that cells may use the same TF to modulate the expression of different genes depending on the TF's nuclear translocation dynamics. Dynamics may then serve the purpose of *multiplexing* information transmission [15]. What matters in this case is whether different external stimuli can be reliably encoded in different dynamics of TF's nuclear fractions allowing their identification [14]. Using information theory and a simple transcription model we found that TF's amplitude and frequency encodings mainly differ in their sensitivity to changes in promoter parameters [16] making frequency modulation better suited for signal identification without requiring other mediators of the transduction. In [16] we studied the information transmission from the TF's nuclear fraction to mRNA production finding that the maximum possible transmission was very similar for amplitude and frequency encodings. In the present Letter we study the differences and similarities between both

encodings when the mapping from the external stimulus to the TF's nuclear dynamics is included in the model. We found that the different way in which amplitude and frequency encoding map external stimuli results in qualitatively different information transmission capabilities: while amplitude encoding is optimal for a limited range of stimuli strengths around a finite value, frequency encoding information transmission improves or remains relatively flat as the stimulus strength increases, provided that the differences between the resulting frequencies are not filtered out by the slower timescales of the subsequent processing. The apparently redundant combination of both mechanisms to encode a type of stimulus can then serve to enlarge the range over which stimulus strengths can be reliably discriminated. In this Letter we discuss one possible such example in *S. cerevisiae* cells.

Expanding signaling capabilities with dynamics [17] is characteristic of the universal second messenger calcium, Ca^{2+} , which encodes different inputs in different spatio-temporal distributions of its free cytosolic concentration [18–20] and differentially regulates gene expression depending on its dynamics [21, 22]. Interestingly, Ca^{2+} is involved in various signaling pathways that result in TF's nuclear fractions pulsatile behaviors [6, 8, 23]. Although TF oscillations might not be a mere reflection of those of intracellular Ca^{2+} , they share some common properties. Sequences of intracellular Ca^{2+} pulses elicited by constant concentrations of external effectors have been observed to be very stochastic in different cell types [24–26]. It was argued [27] that this stochasticity occurs because pulses arise via random Ca^{2+} -channel openings which yield localized Ca^{2+} elevations that eventually nucleate to produce a global increase in Ca^{2+} . This behavior is characteristic of spatially extended excitable systems in which “extreme events” (Ca^{2+} spikes) are triggered by noise and subsequently amplified through space [28, 29]. Intracellular Ca^{2+} patterns have been as-

sociated with excitability [30, 31], several models of Ca^{2+} dynamics are excitable [32, 33] and one of them [33] has been used to study frequency encoding. We briefly remind here that excitable systems are characterized by a stable stationary state and a threshold which, if surpassed due to a perturbation, a long excursion in phase space (a spike) is elicited before the system relaxes to its stable fixed point [34]. Excitability is also characteristic of some pulsatile TFs, *e.g.*, the tumor suppressor, p53, whose nuclear fraction displays non-autonomous “sequences of pulses” [35] that require an excitable network structure for their occurrence [36]. Models of the way in which the TF, Msn2, responds to different stresses in yeast demonstrated that bursts of Msn2 nuclear localization also arise from noise in the signaling pathways [37] and noise-triggered excitable systems have been found to describe correctly differentiation in bacteria [38]. In the case of Ca^{2+} pulses, the interspike time intervals have been observed to be the sum of a fixed component (due to spike duration and refractoriness) and a stochastic one of average, T_{av} , that decreases exponentially with the effector’s concentration [26]. We have recently derived this dependence [39] using a simple model of intracellular Ca^{2+} dynamics in the excitable regime and Kramers law for thermally activated barrier crossing [40]. The exponential dependence is characteristic of noise-driven excitable systems [41] in which the external input increases the noise level or reduces the excitability threshold [42–44]. Interestingly, the TF, Crz1, in yeast exhibits bursts of nuclear localization [6] whose mean frequency can be shown to increase exponentially with extracellular Ca^{2+} . Other TFs that exhibit pulsatile nuclear localization have frequencies that are convex increasing functions of the external stimulus strength [7, 9] and might, in principle, depend exponentially on such strength. Although we have not seen a thorough analysis of this dependence outside Ca^{2+} signaling, based on this discussion, in this Letter we assume that frequency encoding entails an exponential dependence of mean frequency with external input strength as previously done for Ca^{2+} [45].

In this Letter we use the transcription model whose dynamics reduces to [13, 16]:

$$\dot{P}_1 = \frac{k_1[TF]^n}{K_d^n + [TF]^n} - \left(\frac{k_1[TF]^n}{K_d^n + [TF]^n} + d_1 \right) P_1, \quad (1)$$

$$X = N \xrightarrow{\frac{k_2[TF]^n P_1}{K_d^n + [TF]^n}} X = N + 1, X = N \xrightarrow{d_2 X} X = N - 1, \quad (2)$$

where $[TF]$ is the nuclear TF concentration (in dimensionless units), P_1 represents the probability that the promoter is in its active TF-bound state, $X(t)$ is the random number of mRNA molecules at time, t , that can take on the values $N = \{0, 1, 2, \dots\}$ and $k_1 = 1/\text{min}$, $k_2 = 10/\text{min}$, $n = 10$, $K_d = 40$, $d_1 = 0.01/\text{min}$, $d_2 = 0.12/\text{min}$ to guarantee a relatively good informa-

tion transmission for both amplitude and frequency encoding [16]. In all cases, the output is:

$$O = \int_0^T dt X(t), \quad (3)$$

with T the integration time. For amplitude modulation, $[TF]$ is modeled as a single pulse of 10 min duration and (dimensionless) amplitude, $A = A_{TF} + \zeta$, with ζ a noise term and A_{TF} related to the external input strength (the dimensionless concentration of an external ligand), I_{ext} , by a cooperative Hill function:

$$A_{TF}(I_{ext}) = 100 \frac{I_{ext}^h}{I_{ext}^h + EC_{50}^h}, \quad (4)$$

which aggregates in one step the various processes that go from the external stimulus to the TF’s nuclear fraction. For frequency modulation, $[TF]$ is modeled as a sequence of 1 min-duration square pulses of (dimensionless) amplitude 100 plus noise, and interpulse time intervals, $\tau = T_{min} + \eta$, with T_{min} fixed [26] and η an exponentially distributed random variable of rate parameter exponentially dependent on I_{ext} [45] so that $T_{IP} \equiv \langle \tau \rangle$ is:

$$T_{IP}(I_{ext}) = T_{min} (1 + \kappa \exp(-b I_{ext})), \quad (5)$$

with $\kappa, b > 0$. Using an I_{ext} distribution of compact support, $[I_m, I_M]$, we compute numerically the mutual information, MI, between I_{ext} and the mRNA time integral over the 100 min duration of the simulation. We have used $T_{min} = 5, 10 \text{ min}$, various values of κ and, for the I_{ext} distribution either one of these expressions:

$$I_{ext} = x, \quad (6)$$

$$I_{ext} = \exp(4(x - 0.5)) \quad (7)$$

with $0 \leq x \leq 1$ Beta-distributed:

$$f(x) = \frac{x^{\alpha-1}(1-x)^{\beta-1}}{B(\alpha, \beta)}, \quad (8)$$

and different choices of $\alpha, \beta > 1$ s.t. $\alpha + \beta \geq 3$, so to obtain different values for the median and variance of I_{ext} . Choosing Eqs. (6) or (7) the corresponding range of I_{ext} values is spanned “linearly” or “logarithmically”, respectively, with relatively uniform “linear” or “logarithmic” standard deviation as a function of the median. Within those ranges, increasing values of $\alpha + \beta \geq 3$ yield more widely spread medians and standard deviations that are closer together as illustrated in Fig. 1.

We show in Figs. 2 (a),(b) the values, MI, obtained for amplitude encoding using the 10 I_{ext} distributions of Fig. 1 (a), plotting MI as a function of the corresponding medians for different choices of h and EC_{50} in Eq. (4). Qualitatively similar results were obtained for the distributions of Fig. 1 (b) and for other parameter values that yielded more pronounced local maxima in the MI

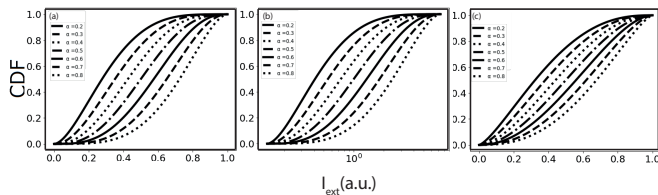


FIG. 1. Cumulative distribution function (CDF) of the stimulus strength, I_{ext} , obtained with Eq. (6) ((a), (c)) and Eq. (7) (b) combined with Eq. (8) for 10 (α, β) pairs such that $\alpha + \beta = 4$ ((a), (b)) and $\alpha + \beta = 6$ ((c)). Varying α and β for increasing values of $\alpha + \beta \geq 3$ yields broader (narrower) ranges of the I_{ext} median (standard deviation).

vs median functions for increasing h or $\alpha + \beta$. We observe in Figs. 2 (a)-(b) that MI is maximum at a median $I_{ext} \leq EC_{50}$ which approaches EC_{50} as h increases and MI remains within a small percent of this maximum for a limited range of medians. This situation is qualitatively different from the one derived for frequency encoding provided that κ and b in Eq. (5) are such that the bulk of the T_{IP} distribution allows the discrimination of nearby mean frequencies (see later) and includes values that are not too long so that the probability of eliciting one pulse during the finite time of the simulation ($100min$) is non-negligible. These two conditions can be satisfied simultaneously, as illustrated in Fig. 2 (c) where we observe that MI can remain close to its maximum value for a broader range of external input strengths than in the case of amplitude encoding. The ability of frequency encoding to distinguish a relatively large range of external input strengths has been observed in pulses of intracellular Ca^{2+} (e.g., distinguishable frequencies elicited in HEK cells by extracellular concentrations of carbachol $\in [30, 200]\mu M$ [26]) and of TF nuclear localization (distinguishable frequencies of the TF, Crz1, in yeast elicited by extracellular $[Ca^{2+}] \in [1, 300]mM$ [6]). We must recall that the finite time of the simulations imposes a limit on the minimum frequency that will likely lead to mRNA production. This limitation is also relevant in physiological situations, due to the finite turn over time of proteins and the need of responses to be generated within a certain time frame. In fact, MI decreases with the median of I_{ext} if the probability of eliciting at least one pulse during the finite observation time becomes too small. This is the case of the examples depicted with solid symbols for which this probability is ~ 0.54 and ~ 0.14 at $I_{ext} = 0.2$ for the cases with $b = 4$ and $b = 6$, respectively. These probabilities are ~ 0.99 and ~ 0.69 for the examples depicted with open symbols and ~ 0.9 for the one with asterisks. As explained later, the decrease of MI with increasing I_{ext} can be attributed to some of the slowest timescales of the transcription model that prevent the discrimination between very short interpulse times.

The different dependence of MI with the median of I_{ext}

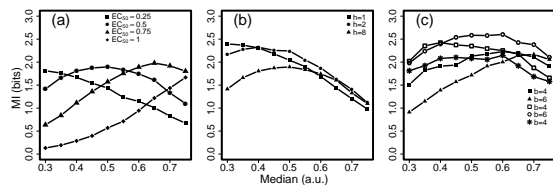


FIG. 2. Mutual Information between O (Eq. (3)) and I_{ext} , for the 10 I_{ext} distributions of Fig. 1 (a) (symbols), as a function of the I_{ext} medians, for amplitude (in (a), (b)) and frequency encoding (in (c)). Eq. (4) was used with $h = 8$ and $EC_{50} = 0.25, 0.5, 0.75, 1$ in (a) and with $EC_{50} = 0.5$ and $h = 1, 2, 8$ in (b). Eq. (5) was used in (c) with $T_{min} = 5min$, $b = 4, 6$ and $\kappa = \exp(b)$ (solid symbols); with $T_{min} = 5min$, and the combinations $b = 4$, $\kappa = 9$ and $b = 6$, $\kappa = e^4$ (open symbols) and with $T_{min} = 10min$, $b = 4$ and $\kappa = 9$ (asterisks).

for amplitude and frequency encoding is due to the different way in which the set of external inputs is “mapped” on the subsequent steps. While a mapping in the form of Eq. (4) only allows to discern a relatively narrow set of external inputs around or below EC_{50} , Eq. (5) can map the whole set of external inputs onto a set of discernible mean interpulse time values. Given two nearby values, I_{ext} and $I_{ext} + \Delta_I$, the first step of the mapping for amplitude encoding will allow their distinction provided that the ratio, Δ_A , between the difference of the corresponding mean TF amplitudes, A_{TF} (Eq. (4)), and the sum of the standard deviations, $2\sigma_\zeta$, satisfies

$$\Delta_A \equiv \frac{\Delta_I}{EC_{50}} \frac{100h}{2\sigma_\zeta} \frac{I_{ext}^{h-1}/EC_{50}^{h-1}}{(I_{ext}^h/EC_{50}^h + 1)^2} > 1, \quad (9)$$

where $\sigma_\zeta = 10$ is the standard deviation of the random variable that is added to A_{TF} in the simulations. In the case of frequency encoding, the resulting interpulse times will be distinguishable provided that the quantiles, p and $1-p$, of the interpulse distributions for I_{ext} and $I_{ext} + \Delta_I$ be further apart. This is satisfied if

$$\Delta_F \equiv \exp(b\Delta_I) \frac{\log(p)}{\log(1-p)} > 1, \quad (10)$$

for some $p > 1/2$ (e.g., $p = 3/4$ guarantees that the overlap of the two distributions does not exceed $1/4$ of the total probability). Eqs. (9) and (10) are qualitatively different: Δ_A is a non-monotone function of I_{ext} , while Δ_F does not depend on I_{ext} . For $h = 8$, the term multiplying Δ_I/EC_{50} in Eq. (9) attains its maximum value at $x \equiv I_{ext}/EC_{50} \approx 1$ and decays by 50% at $x \approx 0.77$ and $x \approx 1.20$. Thus, this first step could distinguish values, I_{ext} , that differ among themselves by $\sim 0.2EC_{50}$ if $0.77 < I_{ext}/EC_{50} < 1.20$. A similar discernment is achieved over the ranges $I_{ext}/EC_{50} \leq 0.4$ for $h = 1$ and $0.17 < I_{ext}/EC_{50} < 1.4$ for $h = 2$. Eq. (10) shows that for large enough b , this step will allow the discernment of nearby input strengths with the same resolution across

the whole range of I_{ext} values. This different behavior is apparent in Fig. 3 where we have plotted the CDFs of TF amplitude, A , (a) and interpulse frequency, $1/\tau$, (b) for each encoding type with a given parameter set of the I_{ext} -TF mapping and 5 I_{ext} distributions whose medians are indicated in the legend. Analyzing Fig. 3 (a) in terms of the MI that is eventually conveyed (curve with solid circles in Fig. 2 (a)) we conclude that the maximum MI (the one with median $I_{ext} = 0.5$) corresponds to the amplitude CDF which is closest to that of a uniform distribution (solid triangles in Fig. 3 (a)). In the case of frequency encoding, almost all the CDFs depicted in Fig. 3 (b) are similarly close to that of a uniform distribution, which could explain the weak dependence of MI with the I_{ext} median for the curve depicted with open squares in Fig. 2 (b). This uniformity resembles the optimal input/output relation derived for cases with small, independent of the mean, noise [46, 47]. This is only the first step in the generation of the response and other uncertainties are subsequently added which further degrade the information. In the case of frequency encoding, too large input strengths can become indistinguishable if the difference between their corresponding mean interpulse times, T_{IP} (Eq. (5)), is so small that it is filtered out by some of the slower processes of the transcription model. Considering that $\Delta T_{IP} \approx \kappa T_{min} \exp(-bI_{ext})b\Delta_I$ for two external inputs, I_{ext} , that differ by Δ_I and that, for the examples with open symbols of Fig. 2 (c) the conditions that yield maximum MI allow their discrimination if they differ by at least $\Delta_I \sim 1/2^{2.5} \approx 0.18$, we estimate that the minimum discernible ΔT_{IP} for these two examples is $\sim 7 - 8min$ which is approximately the characteristic mRNA degradation time of the simulations. We had previously observed that this timescale is key in limiting the information transmitted (see Fig. 3D in [16]). The observation of indistinguishable mean interpulse times in experiments (see *e.g.*, Fig. 4B in [26] or Fig. 3C in [23]) can be used to determine the range of inputs for which frequency encoding can work.

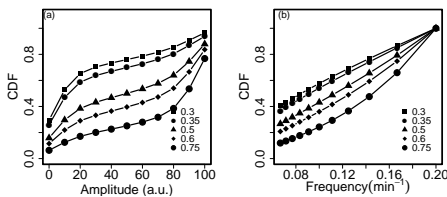


FIG. 3. CDFs of the TF amplitude, A , (a) and of the interpulse frequency, $1/\tau$, (b) derived for 5 of the I_{ext} distributions depicted in Fig. 1 (a) using $EC_{50} = 0.5$ and $h = 8$ in (a) (same parameters as the curve with solid circles in Fig. 2 (a)) and $T_{min} = 5min$, $b = 4$ and $\kappa = 9$ in (b) (same parameters as the curve with open squares in Fig. 2 (c)). The legends indicate the values of the corresponding I_{ext} medians.

The different way in which the two types of strate-

gies encode external stimuli might serve to enlarge the range of distinguishable stimulus strengths in cell types that use the two encodings to respond to the same type of stimulus. This could happen in the yeast mating response [23, 48, 49]. The canonical response of haploid mating type **a** *S. cerevisiae* cells to the pheromone (α -factor) secreted by their potential mating partners, involves amplitude encoding as in Eq. (4) with $h \sim 1$ and dimensional $EC_{50} \approx 3 - 5nM$ [48-50]. Considering that the curve with $h = 1$ in Fig. 2 (b) represents this situation ($[\alpha\text{-factor}] = 6-10nM I_{ext}$ to make the equivalence), we may conclude that MI decreases by ~ 1 bit as the median $[\alpha\text{-factor}]$ increases from 1.8-3 to 3.6-6 nM . Ca^{2+} pulses occur in these cells very rarely for $[\alpha\text{-factor}] = 0$ and their frequency increases with $[\alpha\text{-factor}]$ to values that become indistinguishable for $[\alpha\text{-factor}] > 10nM$ [23]. Although the role of these pulses in the pheromone response pathway is not clear yet, it is conceivable that the transcriptional output be pulsatile as well as it has been observed with the TF, Crz1, in the response to Ca^{2+} stress in yeast [6]. A rough estimate in the form of Eq. (5) derived from Fig. 3C of [23] gives $T_{min} \approx (10 - 12)min$, $\kappa \approx 8 - 9$ and a dimensional $b \sim (0.4 - 0.5)/nM$. Assuming that the curve plotted with asterisks in Fig. 2 (c) ($T_{min} = 10min$, $\kappa = 9$, $b = 4$) corresponds to this situation ($[\alpha\text{-factor}] = (8-10)nM I_{ext}$ to make the equivalence) we conclude that MI differs from its maximum by less than 20% for the whole support of the $[\alpha\text{-factor}]$ distribution, $[0, 8 - 10nM]$. Under physiological conditions, distinguishing relatively subtle differences in $[\alpha\text{-factor}]$ is important for the cell to grow towards the largest $[\alpha\text{-factor}]$ regions to encounter its potential partner. If the partners are apart from one another, we can expect that amplitude encoding be used at the earliest stages of the detection, on one hand, because, as illustrated by the curve with $h = 1$ of Fig. 2 (b), it works correctly for relatively small concentrations (the transition between the behaviors that are characteristic of the absence and presence of pheromone occurs at $[\alpha\text{-factor}] \sim 1nM$ [51]). On the other hand, because if $[\alpha\text{-factor}]$ is too low it will take a relatively long time for an individual cell to collect enough statistics and “respond” correctly using frequency encoding (our estimate of the mean interpulse time derived from [23] yields $\sim 70min$ at $[\alpha\text{-factor}] = 1nM$). Furthermore, there is a time lag between exposing the cells to α -factor and the occurrence of Ca^{2+} pulses which, at the saturating level $[\alpha\text{-factor}] = 100nM$, is of 30min on average [23]. As cells change their form, getting closer to their partners, the pheromone concentration around the growing mating projection gets larger. Amplitude encoding might then cease to discriminate $[\alpha\text{-factor}]$, but frequency encoding could still do its job. Thus, the different range over which each information transmission strategy works properly could be the basis for yeast cells to find their partners when they are close and when they are further apart as well.

ACKNOWLEDGMENTS

This research has been supported by UBA (UBACyT 20020170100482BA) and ANPCyT (PICT 2018-02026 and PICT-2021-III-A-00091).

-
- [1] A. C. Ventura, A. Bush, G. Vasen, M. A. Goldín, B. Burkinshaw, N. Bhattacharjee, A. Folch, R. Brent, A. Chernomoretz, and A. Colman-Lerner, *Proceedings of the National Academy of Sciences* **111**, E3860 (2014), ISSN 0027-8424, <https://www.pnas.org/content/111/37/E3860.full.pdf>, URL <https://www.pnas.org/content/111/37/E3860>.
- [2] M. A. Poritz, S. Malmstrom, M. K. Kim, P. J. Rossmeissl, and A. Kamb, *Yeast* **18**, 1331 (2001).
- [3] R. C. Yu, C. G. Pesce, A. Colman-Lerner, L. Lok, D. Pincus, E. Serra, M. Holl, Benjamin, K. AU-Gordon, Andrew, et al., *Nature* **456**, 755 (2008).
- [4] P. D. Koninck and H. Schulman, *Science* **279**, 227 (1998), <https://www.science.org/doi/pdf/10.1126/science.279.5348.227>, URL <https://www.science.org/doi/abs/10.1126/science.279.5348.227>.
- [5] J. G. Albeck, G. B. Mills, and J. S. Brugge, *Molecular Cell* **49**, 249 (2013).
- [6] L. Cai, C. K. Dalal, and M. B. Elowitz, *Nature* **455**, 485 (2008), ISSN 1476-4687, URL <https://doi.org/10.1038/nature07292>.
- [7] N. Hao and E. K. O'Shea, *Nature Structural & Molecular Biology* **19**, 31 (2012).
- [8] N. Yissachar, T. Sharar Fischler, A. A. Cohen, S. Reich-Zeliger, D. Russ, E. Shifrut, Z. Porat, and N. Friedman, *Mol Cell* **49**, 322 (2012).
- [9] C. Dalal, L. Cai, Y. Lin, K. Rahbar, and M. Elowitz, *Current Biology* **24**, 2189 (2014), ISSN 0960-9822, URL <https://www.sciencedirect.com/science/article/pii/S0960982214009737>.
- [10] F. Tostevin, W. de Ronde, and P. R. ten Wolde, *Phys. Rev. Lett.* **108**, 108104 (2012), URL <https://link.aps.org/doi/10.1103/PhysRevLett.108.108104>.
- [11] G. Micali, G. Aquino, D. M. Richards, and R. G. Endres, *PLOS Computational Biology* **11**, 1 (2015), URL <https://doi.org/10.1371/journal.pcbi.1004222>.
- [12] J. Selimkhanov, B. Taylor, J. Yao, A. Pilko, J. Albeck, A. Hoffmann, L. Tsimring, and R. Wollman, *Science* **346**, 1370 (2014), <https://www.science.org/doi/pdf/10.1126/science.1254933>, URL <https://www.science.org/doi/abs/10.1126/science.1254933>.
- [13] A. S. Hansen and E. K. O'Shea, *Mol Syst Biol* **9**, 704 (2013).
- [14] A. S. Hansen and E. K. O'Shea, *eLife* **4**, e06559 (2015), ISSN 2050-084X, URL <https://doi.org/10.7554/eLife.06559>.
- [15] G. Minas, D. J. Woodcock, L. Ashall, C. V. Harper, M. R. H. White, and D. A. Rand, *PLOS Computational Biology* **16**, 1 (2020), URL <https://doi.org/10.1371/journal.pcbi.1008076>.
- [16] A. Givré, A. Colman-Lerner, and S. Ponce Dawson, *Scientific Reports* **13**, 2652 (2023), URL <https://doi.org/10.1038/s41598-023-29539-3>.
- [17] J. Purvis and G. Lahav, *Cell* **152**, 945 (2013), ISSN 0092-8674, URL <https://www.sciencedirect.com/science/article/pii/S0092867413001530>.
- [18] M. T. Nelson, H. Cheng, M. Rubart, L. F. Santana, A. D. Bonev, H. J. Knot, and W. J. Lederer, *Science* **270**, 633 (1995).
- [19] M. Nishiyama, K. Hong, K. Mikoshiba, M.-m. Poo, and K. Kato, *Nature* **408**, 584 (2000), ISSN 1476-4687, URL <https://doi.org/10.1038/35046067>.
- [20] M. J. Berridge, P. Lipp, and M. D. Bootman, *Nature reviews Molecular cell biology* **1**, 11 (2000).
- [21] R. E. Dolmetsch, K. Xu, and R. S. Lewis, *Nature* **392**, 933 (1998).
- [22] A. E. West, W. G. Chen, M. B. Dalva, R. E. Dolmetsch, J. M. Kornhauser, A. J. Shaywitz, M. A. Takasu, X. Tao, and M. E. Greenberg, *Proceedings of the National Academy of Sciences* **98**, 11024 (2001), <https://www.pnas.org/doi/pdf/10.1073/pnas.191352298>, URL <https://www.pnas.org/doi/abs/10.1073/pnas.191352298>.
- [23] N. Carbó, N. Tarkowski, E. P. Ipiña, S. P. Dawson, and P. S. Aguilar, *Molecular Biology of the Cell* **28**, 501 (2017), <http://www.molbiolcell.org/content/28/4/501.full.pdf+html>, URL <http://www.molbiolcell.org/content/28/4/501.abstract>.
- [24] A. Skupin, H. Kettenmann, U. Winkler, M. Wartenberg, H. Sauer, S. C. Tovey, C. W. Taylor, and M. Falcke, *Biophys. J.* **94**, 2404 (2008).
- [25] S. Dragoni, U. Laforenza, E. Bonetti, F. Lodola, C. Bottino, R. Berra-Romani, G. Carlo Bongio, M. P. Cinelli, G. Guerra, P. Pedrazzoli, et al., *STEM CELLS* **29**, 1898 (2011), <https://stemcellsjournalsonline.wiley.com/doi/pdf/10.1002/stem.734>, URL <https://stemcellsjournalsonline.wiley.com/doi/abs/10.1002/stem.734>.
- [26] K. Thurley, S. C. Tovey, G. Moenke, V. L. Prince, A. Meena, A. P. Thomas, A. Skupin, C. W. Taylor, and M. Falcke, *Science Signaling* **7**, ra59 (2014), ISSN 1945-0877, <http://stke.sciencemag.org/content/7/331/ra59.full.pdf>, URL <http://stke.sciencemag.org/content/7/331/ra59>.
- [27] K. Thurley and M. Falcke, *Proceedings of the National Academy of Sciences* **108**, 427 (2011), ISSN 0027-8424, <http://www.pnas.org/content/108/1/427.full.pdf>, URL <http://www.pnas.org/content/108/1/427>.
- [28] L. Lopez, E. Piegari, L. Sigaut, and S. Ponce Dawson, *Frontiers in Physiology* **3** (2012), ISSN 1664-042X, URL http://www.frontiersin.org/fractal_physiology/10.3389/fphys.2012.00350/abstract.
- [29] L. Hernández-Navarro, S. Faci-Lázaro, J. G. Orlandi, U. Feudel, J. Gómez-Gardeñes, and J. Soriano, *Phys. Rev. Res.* **3**, 023133 (2021), URL <https://link.aps.org/doi/10.1103/PhysRevResearch.3.023133>.
- [30] J. Lechleiter, S. Girard, E. Peralta, and D. Clapham, *Science* **252**, 123 (1991), <https://www.science.org/doi/pdf/10.1126/science.2011747>, URL <https://www.science.org/doi/abs/10.1126/science.2011747>.
- [31] J. D. Lechleiter and D. E. Clapham, *Cell* **69**, 283 (1992), ISSN 0092-8674, URL <https://www.sciencedirect.com/science/article/pii/S0092867492904096>.

- [32] Y.-X. Li and J. Rinzel, *Journal of Theoretical Biology* **166**, 461 (1994), ISSN 0022-5193, URL <https://www.sciencedirect.com/science/article/pii/S0022519384710411>.
- [33] Y. Tang and H. G. Othmer, *Proceedings of the National Academy of Sciences* **92**, 7869 (1995), ISSN 0027-8424, <http://www.pnas.org/content/92/17/7869.full.pdf>, URL <http://www.pnas.org/content/92/17/7869>.
- [34] E. M. IZHIKEVICH, *International Journal of Bifurcation and Chaos* **10**, 1171 (2000), <https://doi.org/10.1142/S0218127400000840>, URL <https://doi.org/10.1142/S0218127400000840>.
- [35] E. Batchelor, C. S. Mock, I. Bhan, A. Loewer, and G. Lahav, *Molecular Cell* **30**, 277 (2008), ISSN 1097-2765, URL <https://www.sciencedirect.com/science/article/pii/S1097276508002402>.
- [36] G. Mönke, E. Cristiano, A. Finzel, D. Friedrich, H. Herzel, M. Falcke, and A. Loewer, *Scientific Reports* **7**, 46571 (2017), URL <https://doi.org/10.1038/srep46571>.
- [37] N. Petrenko, R. V. Chereji, M. N. McClean, A. V. Morozov, and J. R. Broach, *Mol Biol Cell* **24**, 2045 (2013).
- [38] A. Eldar and M. B. Elowitz, *Nature* **467**, 167 (2019), URL <https://doi.org/10.1038/nature09326>.
- [39] A. Givré and S. P. Dawson, *Cell information processing via frequency encoding and excitability* (2023), 2312.17629.
- [40] P. Hänggi, P. Talkner, and M. Borkovec, *Rev. Mod. Phys.* **62**, 251 (1990), URL <https://link.aps.org/doi/10.1103/RevModPhys.62.251>.
- [41] B. Lindner, J. García-Ojalvo, A. Neiman, and L. Schimansky-Geier, *Physics Reports* **392**, 321 (2004), ISSN 0370-1573, URL <http://www.sciencedirect.com/science/article/pii/S0370157303004228>.
- [42] C. B. Muratov, E. Vanden-Eijnden, and W. E., *Physica D: Nonlinear Phenomena* **210**, 227 (2005), ISSN 0167-2789, URL <https://www.sciencedirect.com/science/article/pii/S0167278905003155>.
- [43] R. E. Lee DeVille, E. Vanden-Eijnden, and C. B. Muratov, *Phys. Rev. E* **72**, 031105 (2005), URL <https://link.aps.org/doi/10.1103/PhysRevE.72.031105>.
- [44] M. C. Eguia and G. B. Mindlin, *Phys Rev E Stat Phys Plasmas Fluids Relat Interdiscip Topics* **61**, 6490 (2000).
- [45] A. Givré and S. Ponce Dawson, *Frontiers in Physics* **6** (2018), ISSN 2296-424X, URL <https://www.frontiersin.org/articles/10.3389/fphy.2018.00074>.
- [46] S. Laughlin, *Zeitschrift für Naturforschung C* **36**, 910 (1981), URL <https://doi.org/10.1515/znc-1981-9-1040>.
- [47] W. Bialek, *Reports on Progress in Physics* **81**, 012601 (2017), URL <https://dx.doi.org/10.1088/1361-6633/aa995b>.
- [48] T.-M. Yi, H. Kitano, and M. I. Simon, *Proceedings of the National Academy of Sciences* **100**, 10764 (2003), ISSN 0027-8424, <https://www.pnas.org/content/100/19/10764.full.pdf>, URL <https://www.pnas.org/content/100/19/10764>.
- [49] A. Bush, G. Vasen, A. Constantinou, P. Dunayevich, I. L. Patop, M. Blaustein, and A. Colman-Lerner, *Molecular Systems Biology* **12**, 898 (2016), <https://www.embopress.org/doi/pdf/10.15252/msb.20166910>, URL <https://www.embopress.org/doi/abs/10.15252/msb.20166910>.
- [50] A. Colman-Lerner, A. Gordon, E. Serra, T. Chin, O. Resnekov, D. Endy, C. Gustavo Pesce, and R. Brent, *Nature* **437**, 699–706 (2005), URL <https://www.nature.com/articles/nature03998>.
- [51] N. Muller, M. Piel, V. Calvez, R. Voituriez, J. Gonçalves-Sá, C.-L. Guo, X. Jiang, A. Murray, and N. Meunier, *PLOS Computational Biology* **12**, 1 (2016), URL <https://doi.org/10.1371/journal.pcbi.1004795>.